PHYSICS

Intrinsic magnetic topological insulators in van der Waals layered $MnBi_2Te_4$-family materials

Jiaheng Li[1,2], Yang Li[1,2], Shiqiao Du[1,2], Zun Wang[1,2], Bing-Lin Gu[1,2,3], Shou-Cheng Zhang[4]*, Ke He[1,2]†, Wenhui Duan[1,2,3]†, Yong Xu[1,2,5]†

The interplay of magnetism and topology is a key research subject in condensed matter physics, which offers great opportunities to explore emerging new physics, such as the quantum anomalous Hall (QAH) effect, axion electrodynamics, and Majorana fermions. However, these exotic physical effects have rarely been realized experimentally because of the lack of suitable working materials. Here, we predict a series of van der Waals layered $MnBi_2Te_4$-related materials that show intralayer ferromagnetic and interlayer antiferromagnetic exchange interactions. We find extremely rich topological quantum states with outstanding characteristics in $MnBi_2Te_4$, including an antiferromagnetic topological insulator with the long-sought topological axion states on the surface, a type II magnetic Weyl semimetal with one pair of Weyl points, as well as a collection of intrinsic axion insulators and QAH insulators in even- and odd-layer films, respectively. These notable predictions, if proven experimentally, could profoundly change future research and technology of topological quantum physics.

INTRODUCTION

The correlation between topology and symmetry as a central fundamental problem of modern physics has attracted intensive research interests in condensed matter physics and materials science since the discovery of topological insulators (TIs) (*1*, *2*). One essential symmetry is the time-reversal symmetry (TRS), which is crucial to many kinds of topological quantum states of matter such as TIs and is broken in the presence of magnetism. Intriguingly, the interplay between magnetism and topology could generate a variety of exotic topological quantum states in materials (*1*–*23*), including the quantum anomalous Hall (QAH) effect, showing dissipationless chiral edge states (*3*–*6*), the topological axion states, displaying quantized magnetoelectric effects (*7*–*10*), and Majorana fermions, obeying non-Abelian statistics (*2*, *11*). In this context, great research effort has been devoted to exploring exotic topological quantum physics, which is of profound importance to fundamental science and future technologies, such as dissipationless topological electronics and topological quantum computation (*1*, *2*).

One key subject that is of crucial significance to the whole research community is the development of topological quantum materials (TQMs) showing the coexistence of topology and other quantum phases (e.g., magnetism, ferroelectricity, charge density wave, and superconductivity), coined "composite TQMs" (CTQMs), which include magnetic TQMs (MTQMs) as an important subset. Currently, a very limited number of MTQMs are experimentally available, including magnetically doped TIs and magnetic topological heterostructures (*5*, *6*, *24*–*31*), whose material fabrication, experimental measurement, and property optimization are quite challenging. Because the major topological properties of these existing MTQMs depend sensitively on delicate magnetic doping or proximity effects, only little preliminary experimental progress has been achieved until now, leaving many important physical effects not ready for practical use or still unproved. For instance, the QAH effect was only observed in magnetically doped $(Bi_xSb_{1-x})_2Te_3$ thin films at very low working temperatures by fine-tuning chemical compositions (*5*, *6*). While a previous theory predicted the existence of topological axion states at the surface of a three-dimensional (3D) antiferromagnetic (AFM) TI (*10*), the 3D AFM TI phase has not been realized experimentally, as far as we know, despite several attempts. For future research and applications, people should go beyond the existing strategy for building MTQMs and try to design intrinsic MTQMs without the need of introducing alloy/doping or heterostructures.

Noticeably, van der Waals (vdW) layered materials represent a large family of materials with greatly tunable properties by quantum size effects or vdW heterojunctions (*32*), in which a variety of quantum phases in different spatial dimensions have been discovered by state-of-the-art research (*21*, *33*, *34*). For instance, TI states were previously found in the tetradymite-type Bi_2Te_3-class materials (*33*), and 2D intrinsic magnetism was recently found in ultrathin films of CrI_3 (*35*) and $Cr_2Ge_2Te_6$ (*36*) . However, these topological materials are not magnetic, and those magnetic materials are not topological. It is highly desirable to incorporate magnetic and topological states together into the same vdW material to obtain layered intrinsic MTQMs, which are able to inherit advantages of vdW materials.

RESULTS

In this work, on the basis of first-principles density functional theory (DFT) calculations, we predicted a series of layered intrinsic MTQMs from the tetradymite-type $MnBi_2Te_4$-related ternary chalcogenides (MB_2T_4: M = transition-metal or rare-earth element, B = Bi or Sb, T = Te, Se, or S) (Fig. 1A), in which the intralayer exchange coupling is ferromagnetic (FM), giving 2D ferromagnetism in the monolayer, while the interlayer exchange coupling is AFM, forming 3D *A*-type antiferromagnetism in their vdW layered bulk. Both 2D and 3D physics are easily accessible in this family of materials by varying film thickness. Moreover, magnetic states are tunable from AFM to FM

[1]State Key Laboratory of Low Dimensional Quantum Physics, Department of Physics, Tsinghua University, Beijing 100084, People's Republic of China. [2]Collaborative Innovation Center of Quantum Matter, Beijing 100084, People's Republic of China. [3]Institute for Advanced Study, Tsinghua University, Beijing 100084, People's Republic of China. [4]Stanford Center for Topological Quantum Physics, Stanford University, Stanford, CA 94305-4045, USA. [5]RIKEN Center for Emergent Matter Science (CEMS), Wako, Saitama 351-0198, Japan.
*Deceased
†Corresponding author. Email: kehe@tsinghua.edu.cn (K.H.); dwh@phys.tsinghua.edu.cn (W.D.); yongxu@mail.tsinghua.edu.cn (Y.X.)

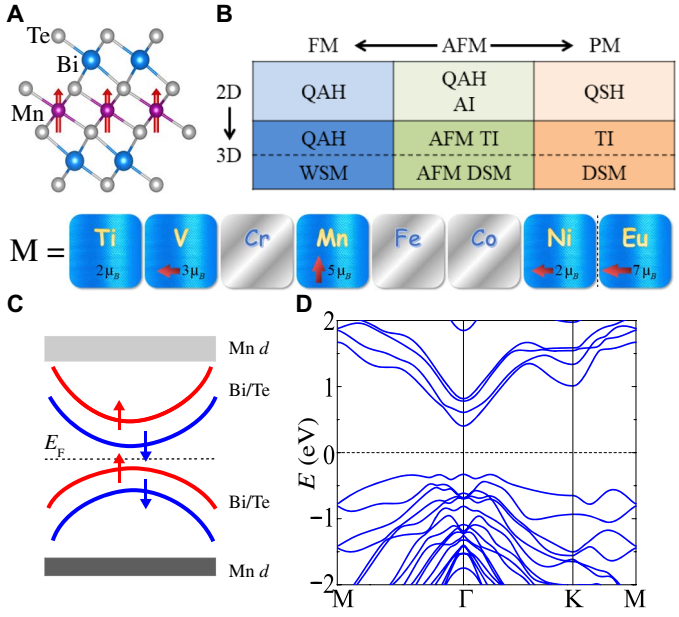

Fig. 1. The MB_2T_4-family materials (MB_2T_4: M = transition-metal or rare-earth element, B = Bi or Sb, T = Te, Se, or S) using $MnBi_2Te_4$ as an example. (**A**) Monolayer MB_2T_4 with an FM M layer, whose easy axis is out of plane for MB_2T_4. The monolayer is predicted to be an FM insulator for varying element M (blue panels). It is metallic and possibly unstable for other elements (gray panels). The total magnetic moments per unit cell and their orientations (out of plane or in plane) of MBi_2Te_4 are depicted by the numbers and red arrows, respectively, in the bottom panel. Note that the magnetic easy axis is unknown for M = Ti. (**B**) Rich topological quantum states in MB_2T_4 thin films (2D) and bulks (3D) of different magnetic states that are tunable from AFM to FM or PM. AI, axion insulator; QSH, quantum spin Hall; DSM, Dirac semimetal. (**C**) Schematic diagram showing that magnetism and topology in $MnBi_2Te_4$ are induced by Mn *d*-bands and Bi-Te *p*-bands, respectively. (**D**) Band structure of monolayer $MnBi_2Te_4$, which is an FM insulator.

under external magnetic fields or to paramagnetic (PM) at high temperatures, leading to different symmetry properties and thus distinct topological quantum states. Therefore, these materials provide a promising platform to investigate the interplay of dimension, symmetry, magnetism, and topology, as illustrated in Fig. 1B. They could host many unusual 2D and 3D topological quantum states, including QAH insulators (*4*–*6*), axion insulators (*7*–*9*), and quantum spin Hall insulators (*37*–*39*) in the thin films, as well as 3D QAH insulators (*12*), Weyl semimetals (WSMs) (*17*–*21*), Dirac semimetals (*22*, *23*), time-reversal invariant TIs (*33*), and AFM TIs (*10*) in the bulk. We demonstrated that almost all of those exotic physical effects could be realized in the representative material $MnBi_2Te_4$. As the bulk and thin films of this particular material have been successfully fabricated experimentally (*40*, *41*), our theoretical predictions are awaiting experimental proofs.

The tetradymite-type $MnBi_2Te_4$ crystalizes in a rhombohedral layered structure with the space group $R\bar{3}m$ (*40*, *42*), and each layer has a triangular lattice with atoms ABC stacked along the out-of-plane direction, the same as Bi_2Te_3. Slightly differently, monolayer $MnBi_2Te_4$ includes seven atoms in a unit cell, forming a Te-Bi-Te-Mn-Te-Bi-Te septuple layer, which can be viewed as intercalating a Mn-Te bilayer into the center of a Bi_2Te_3 quintuple layer (Fig. 1A). Noticeably, the mixing between Mn and Bi in this compound would create unstable valence states Mn^{3+} and Bi^{2+}, which is energetically unfavorable. Thus, the formation of alloys could be avoided, leading to a stoichiometric compound. This physical mechanism also explains the stability of compounds such as $SnBi_2Te_4$ and $PbBi_2Te_4$ and is applicable to many other $MnBi_2Te_4$-family materials. Our DFT calculations predicted that a series of $MnBi_2Te_4$ compounds are dynamically stable (at least metastable), including M = Ti, V, Mn, Ni, Eu, etc. (Fig. 1A), as confirmed by DFT phonon calculations (Supplementary Materials), implying that these materials could possibly be fabricated by experiment. These stable compounds are characterized by an insulating band gap in their single layers, offering a collection of layered intrinsic magnetic (topological) insulators. Comprehensive data on the atomic, magnetic, and electronic properties of MBi_2Te_4-family materials were presented in the Supplementary Materials.

In $MnBi_2Te_4$, Mn has a valence of +2 by losing its two 4*s* electrons. The remaining five 3*d* electrons fill up the spin-up Mn-*d* levels according to the Hund's rule, introducing 5 μ_B magnetic moment (mostly from Mn) per unit cell. By comparing different magnetic structures, we found that the magnetic ground state of the monolayer is FM with an out-of-plane easy axis (depicted in Fig. 1A), in agreement with previous work (*30*). Each Mn atom is bonded with six neighboring Te atoms, which form a slightly distorted edge-sharing octahedron. According to the Goodenough-Kanamori rule, the superexchange interactions between Mn-Te-Mn with a bonding angle of ~86° are FM, similarly as in CrI_3 and $Cr_2Ge_2Te_6$ (*35*, *36*). We found that intralayer exchange couplings are FM in other stable MB_2T_4-family members, but the magnetic easy axis can be varied to in-plane (e.g., for M = V), displaying rich 2D magnetic features (Fig. 1A).

Intriguingly, magnetic and topological states are well combined in $MnBi_2Te_4$, where Mn introduces magnetism and the Bi-Te layers could generate topological states similarly as in Bi_2Te_3 (*33*), as schematically depicted in Fig. 1C. The spin splitting between spin-up and spin-down Mn *d* bands is extremely large (>7 eV) because of the large magnetic moment of Mn. Thus, Mn *d*-bands are far away from the band gap, and only Bi/Te *p*-bands are close to the Fermi level. While the monolayer is a topologically trivial FM insulator with a direct band gap of 0.70 eV (Fig. 1D), extremely interesting topological quantum physics emerges in the bulk and thin films. Note that monolayer $MnBi_2Te_4$ was introduced as an FM insulator to break the TRS of a TI surface to realize the QAH and topological magnetoelectric effects in the magnetic topological heterostructures (*30*, *31*). Topological properties of $MnBi_2Te_4$ itself, however, were not discussed.

We found that the interlayer magnetic coupling is AFM, giving an *A*-type AFM ground state (depicted in Fig. 2A) (*41*), which is similar to that in CrI_3 (*35*) and is explained by the interlayer super-superexchange coupling. In the AFM bulk, the spatial inversion symmetry *P* (i.e., P_1 centered at O_1) is preserved, but the TRS Θ gets broken. Two new symmetries exist: $P_2\Theta$ and $S = \Theta T_{1/2}$, where P_2 is an inversion operation centered at O_2 and $T_{1/2}$ is a lattice translation (depicted in Fig. 2A). The band structures with and without spin-orbit coupling (SOC) are presented in Fig. 2 (B and C). Here, every band is (at least) doubly degenerate, which is ensured by $P_2\Theta$ (*22*). In the presence of *S*, a Z_2 classification becomes feasible (*10*). However, in contrast to the time-reversal invariant case, there is a Z_2 invariant for the $k_z = 0$ plane but not for the $k_z = \pi$ plane. Here, $Z_2 = 1$ corresponds to a 3D AFM TI phase (*10*), which has not been experimentally confirmed before.

Here, the parity criteria can be applied to determine Z_2 due to the P_1 symmetry (*43*). The parities of the valence band maximum and

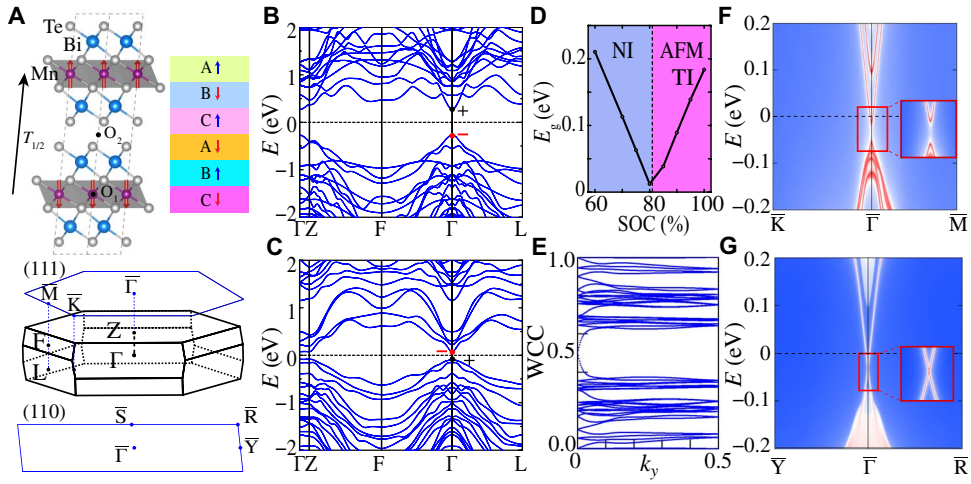

Fig. 2. AFM $MnBi_2Te_4$ bulk. (**A**) Crystal structure (top left) and Brillouin zones of bulk, (111), and (110) surfaces (bottom) of ABC-stacked $MnBi_2Te_4$ with an *A*-type AFM ordering (top right). O_1 and O_2 represent inversion centers, and $T_{1/2}$ denotes a lattice translation. (**B** and **C**) Band structures excluding (B) and including (C) SOC. Parities of Bloch wave functions at Γ are labeled by "+" and "–." (**D**) Band gap at Γ as a function of the SOC strength. The system would vary from normal insulator (NI) to AFM TI if gradually turning on SOC. (**E**) Evolution of WCCs in the $k_z = 0$ plane, which implies a nonzero topological invariant. (**F** and **G**) Surface states of the semi-infinite (111) (F) and (110) (G) surfaces, which are gapped and gapless, respectively.

conduction band minimum at Γ are opposite, and both change signs by the SOC effects (Fig. 2, B and C), implying a band inversion. By varying the SOC strength, the band gap first closes and then reopens at Γ (Fig. 2D), showing one band inversion and thus implying a topological phase transition. The SOC-induced band reversal happens between Bi p_z^+ and Te p_z^-, essentially the same as for Bi_2Te_3 (*33*). Our Wannier charge center (WCC) calculations for the $k_z = 0$ plane revealed that $Z_2 = 1$ when including SOC (Fig. 2E), confirming that $MnBi_2Te_4$ is a 3D AFM TI. The global band gap is direct at *Z* (~0.16 eV), and the direct gap at Γ is ~0.18 eV. One prominent feature of the AFM TI is the existence of 2D gapless surface states at side surfaces that have preserved *S* symmetry, which is confirmed by the surface-state calculations (Fig. 2, F and G). The surface states are gapless on the (110) termination, showing Rashba-like spin textures (fig. S5B), but become gapped on the (111) termination due to the *S* symmetry breaking, in agreement with previous theory (*10*).

The intrinsically gapped (111) surfaces are promising for probing the long-sought topological axion states, which give the topological quantized magnetoelectric effects related to an axion field with $\theta = \pi$ (*7*–*10*). Previous works proposed to probe the axion states by adding opposite out-of-plane ferromagnetism onto the bottom and top surfaces of 3D TIs (*7*, *25*–*27*) or by applying magnetic fields on TI films (*44*). These TRS-broken surface states are naturally and intrinsically provided by even-layer $MnBi_2Te_4$ films (when with negligible hybridizations between the top and bottom surface states), benefitting from their *A*-type AFM states. An additional requirement is to open a band gap at side surfaces, which is realized in relatively thin films [~10 layers according to a simple estimation (Supplementary Materials)] or by applying magnetic fields that have nonzero components perpendicular to all side surfaces. The simplified proposal, together with the suitable material candidate $MnBi_2Te_4$, could greatly facilitate the research of axion electrodynamics.

As the interlayer exchange coupling is quite weak here, the AFM ground state of $MnBi_2Te_4$ could be tuned, for instance, by applying an external magnetic field, to other magnetic configurations. Then, the material symmetry changes, leading to distinct topological phases. This concept is demonstrated by studying a simple FM ordering along the out-of-plane direction (Fig. 3A). The FM bulk has P_1 but neither Θ nor $P_2\Theta$, leading to spin-split bands, nonzero Berry curvatures, and possibly nonzero topological Chern numbers that correspond to nontrivial topological phases, such as 3D QAH insulators (*12*) and WSMs (*17*–*21*). The band structure of FM $MnBi_2Te_4$ bulk (Fig. 3B) displays a pair of band crossings at W/W′ along the $\bar{Z}$-Γ-Z line (Fig. 3C). The band crossings are induced by interlayer orbital hybridizations and protected by the C_3 rotational symmetry. Our WCC calculations found that the W point is a momentum-space monopole with a topological charge of +1 (i.e., a Berry phase of 2π) (Fig. 3D), and its time-reversal partner W′ has an opposite topological charge of −1, indicating that the system is a topological WSM. While in most of momentum space the electron pocket is located above the hole pocket (e.g., along the F-W-L line), the Weyl cones get tilted along the $\bar{Z}$-Γ-Z line (Fig. 3C), leaving some parts of the electron pocket below the hole pocket, which is the characteristic feature of type II WSMs (*21*). In contrast to the time-reversal invariant WSMs that must have even pairs of Weyl points, this magnetic WSM represents the simplest one, hosting only a pair of Weyl points. Moreover, our surface-state calculations demonstrated the existence of Fermi arcs on the $(1\bar{1}0)$ termination (Fig. 3E), which is the fingerprint of WSMs. These two Weyl points are well separated in momentum space and very close to the Fermi level, advantageous for experimental observations. Thin films of magnetic WSMs typically give the QAH effect, which will be discussed later.

VdW layered materials are featured by tunable quantum size effects. For AFM $MnBi_2Te_4$ films, even layers do not possess *P* and Θ symmetries but have $P_2\Theta$, ensuring double degeneracy in every band (*22*). Differently, odd layers have *P* but neither Θ nor $P_2\Theta$, leading to spin-split bands. Different symmetries in even and odd layers lead to distinct topological properties. Specifically, the topological Chern number $C = 0$ is required by $P_2\Theta$ in even layers, but $C \neq 0$ is allowed in odd layers. In contrast to the single- and three-layer films, where a trivial insulating gap is opened by quantum confinement effects, we found that the five-layer film is an intrinsic QAH

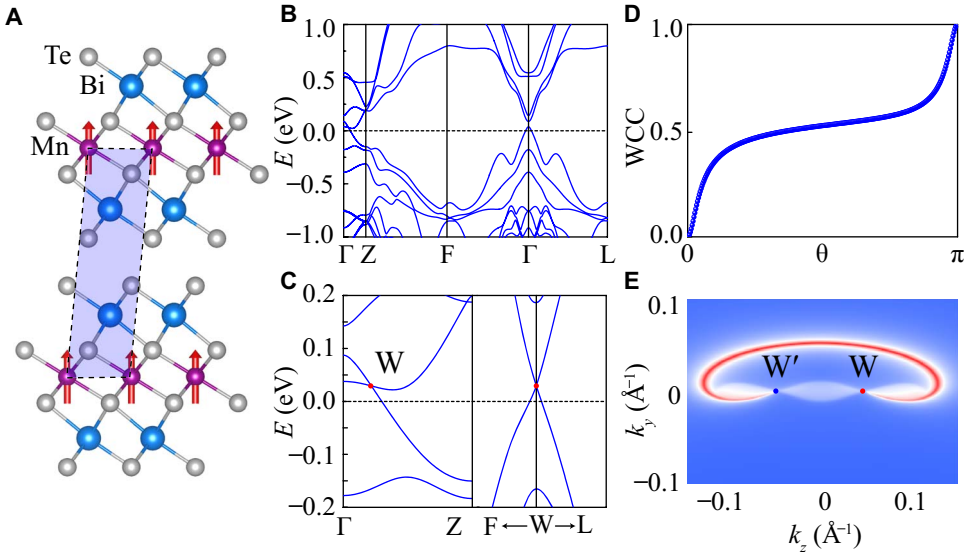

Fig. 3. FM $MnBi_2Te_4$ bulk. Crystal structure (**A**) and band structure (**B**) of the FM bulk. (**C**) Zoom-in band structures along the out-of-plane Γ-Z and nearly in-plane F-W-L directions. There is a pair of Weyl points at W and W′ = −W. (**D**) Motion of the sum of WCCs on a small sphere centered at W in momentum space. (**E**) Surface states of the $(1\bar{1}0)$ termination on the isoenergy plane of the Weyl points, demonstrating the existence of Fermi arcs.

insulator with $C = 1$, as confirmed by the appearance of a quantized Hall conductance and chiral edge states within the bulk band gap (Fig. 4, A to C). We also calculated a seven-layer film, which is also a QAH insulator with $C = 1$. For comparison, our calculations of a four-layer film show that there is no gapless edge states within the bulk gap, confirming that $C = 0$ for an even-layer film (Supplementary Materials).

Exchange splitting introduced by the magnetic Mn layers, together with the strong SOC effects in the Bi-Te bands, cooperatively induces the QAH effect, similarly as in the magnetically doped Bi_2Te_3-class TIs (*4*). However, the present material has an intrinsic magnetism and does not need uncommon mechanisms [e.g., the Van-Vleck mechanism (*4*)] to induce ferromagnetism in insulating states. Moreover, because the magnetic doping is not needed, disorder-induced magnetic domains and potential fluctuations, which deteriorate the QAH effect, are avoided. Furthermore, the QAH gap of the five-layer film is 38 meV, greater than the room temperature thermal energy of 26 meV, enabling a high working temperature.

The thickness dependence behaviors of films are illustrated in Fig. 4 (D and E). There are intrinsically gapped surface states on both sides of thick films, as obtained for the (111) semi-infinite surface. These surface gaps are opened by the TRS-breaking field near the surface, which have half-quantized Hall conductances $\sigma_{xy} = e^2/2h$ or $-e^2/2h$ when the magnetism in the surface layer is up- or down-oriented, respectively. Thus, the Hall conductances of the top and bottom surfaces are cancelled in even layers, giving axion insulators with $C = 0$ or topological axion states mentioned above (Fig. 4D), while they get added in odd layers, giving QAH insulators with $C = 1$ (Fig. 4E). This physical picture, consistent with our calculation results, suggests an oscillation of C in even and odd layers. Thus, chiral edge states always appear near step edges (Fig. 4F), which can be used for dissipationless conduction. On the basis of this unique feature, chiral edge states could be selectively patterned in the present material by controlling the film thickness or step edges, advantageous for building dissipationless circuits.

DISCUSSION

Experimentally, the material is not intrinsically insulating due to the existence of dopants, but the Fermi level should be tuned to the bulk gap for observing the QAH and topological magnetoelectric effects. This could be realized by various techniques, such as alloying between $MnBi_2Te_4$ and $MnSb_2Te_4$ or ionic liquid gating. Moreover, defects in AFM materials could lead to uncompensated magnetic moment and localized spin canting. The effect, however, is usually localized and disordered, which hardly changes the global topological property. Another crucial issue is the influence of temperature on topological properties. The observation of magnetic topological effects depends crucially on the existence of surface gap induced by magnetization. When some spins are flipped due to thermal excitation, the net magnetization of surfaces becomes smaller, which decreases the topological surface gap. If the temperature is gradually increased, the magnetic configuration would change from AFM to PM at ~20 K in the $MnBi_2Te_4$ thin film (*41*), leading to a topological phase transition from AFM TI to TRS invariant TI. The latter phase has gapless surface states. Therefore, the emergence of magnetization-induced surface gap with decreasing temperature provides a smoking gun signature for the temperature-driven topological phase transition.

Looking back to the history of the TI research, the first- and second-generation TIs are the HgTe/CdTe quantum wells (*38*, *39*) and Bi-Sb alloys (*43*, *45*, *46*), respectively, which are very complex and difficult to study theoretically and experimentally. Research interests have increased exponentially since the discovery of the third-generation TIs in the intrinsic Bi_2Te_3-class materials (*33*). A very similar situation is faced by the research of magnetic topological physics. Currently, experimental works are mostly based on magnetically doped TIs (*5*, *6*) and magnetic topological heterostructures (*25*–*31*), which are quite challenging and have led to little preliminary progress. Looking forward, the research progress is expected to be greatly prompted by discovering intrinsic MTQMs that are simple and easy to control. The vdW layered $MnBi_2Te_4$-family materials satisfy all these material traits. This material class could host extremely rich topological

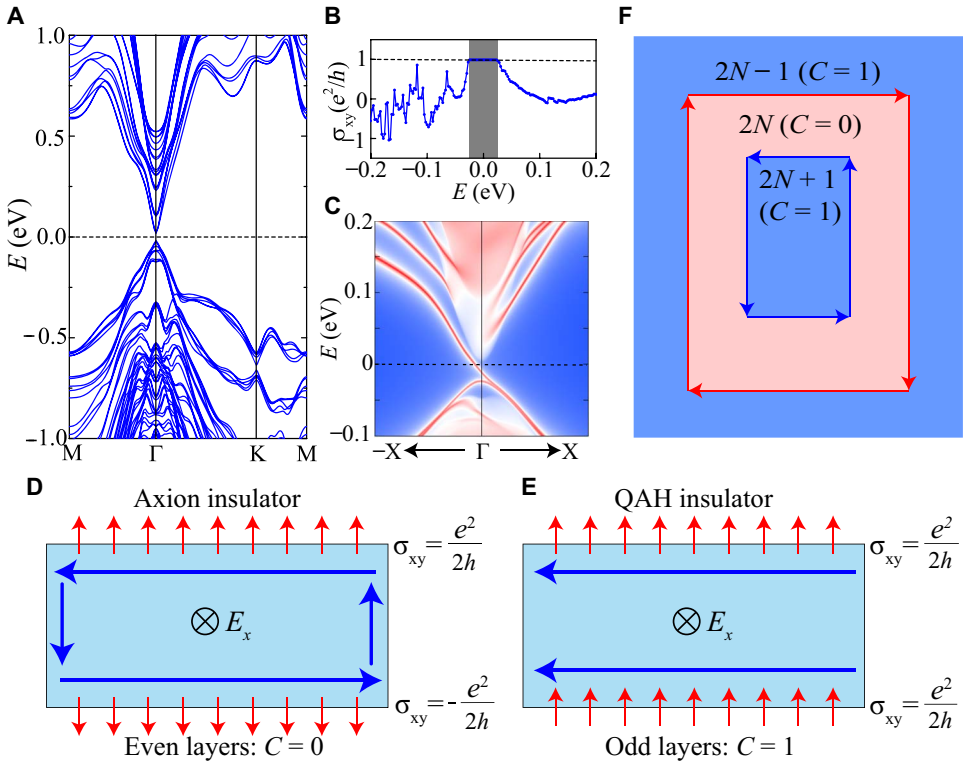

Fig. 4. AFM $MnBi_2Te_4$ films. Band structure (**A**), Hall conductance σ_{xy} (**B**), and edge states (**C**) of the five-layer film. (**D** and **E**) Illustration of intrinsic axion insulators in even layers and QAH insulators in odd layers. The intrinsically gapped surfaces on the top and bottom sides have half-quantized Hall conductances, whose signs are opposite (the same) in even (odd) layers, leading to $C = 0$ ($C = 1$). In even layers, an electric field could induce magnetization effects identical to the depicted circulating Hall current, showing quantized magnetoelectric effects. (**F**) Schematic diagram showing chiral edge states on step edges between even ($2N$) and odd ($2N + 1$) layers.

quantum states in different spatial dimensions and is also promising for investigating other exotic emerging physics (such as Majorana fermions if interacting with superconductivity), which thus could serve as a next-generation material platform for future research.

Note that, after posting the preprint of this work (arXiv:1808.08608) online, we became aware of related works on $MnBi_2Te_4$ bulk (*47*, *48*), $MnBi_2Te_4$ thin films (*41*, *49*), and the $MnBi_2Se_4$ counterparts (*50*), as well as the intrinsic anomalous Hall effect (*51*) and topological superconductivity (*52*) in the same material.

METHODS

First-principles DFT calculations were mainly performed with the Vienna Ab initio Simulation Package (VASP) (*53*) using the projector-augmented wave method and the plane-wave basis with an energy cutoff of 350 eV. The Perdew-Burke-Ernzerhof (PBE) exchange-correlation functional (*54*) was used in combination with the GGA+*U* method to treat the localized *d* and *f* orbitals. The *U* parameter was tested and selected to be $U = 3$, 3, 4, 4, and 5 eV for 3*d* or 4*f* orbitals of Ti, V, Mn, Ni, and Eu, respectively. In addition, the Heyd-Scuseria-Ernzerhof (HSE) hybrid functional (*55*) and the modified Becke-Johnson (mBJ) functional (*56*) were used. The structural optimization and phonon calculations were done by the GGA+*U* method. vdW corrections were included by the DFT-D3 method (*57*) when studying few-layer films or bulks. Band structures of AFM and FM $MnBi_2Te_4$ bulks were computed by the GGA+*U* and mBJ methods, respectively, whose results were further verified by the more advanced HSE method. Electronic bands of monolayer structures were calculated by the HSE functional to correct the band gap problem by using the all-electron, full-potential code FHI-aims (*58*). The Monkhorst-Pack *k*-point meshes of $9 \times 9 \times 3$, $9 \times 9 \times 5$, and $12 \times 12 \times 1$ were adopted for the calculations of AFM bulk, FM bulk, and monolayer/few-layer structures, respectively. The dense Monkhorst-Pack *k*-point meshes of $24 \times 24 \times 1$ were used to calculate magnetocrystalline anisotropy energies of monolayer MB_2T_4. Structure optimizations were performed with a force criterion of 0.01 eV/A. Phonon dispersions were calculated by the frozen phonon method using $3 \times 3 \times 1$ supercells. Surface- and edge-state calculations based on maximally localized Wannier functions were done using the WannierTools package (*59*).

SUPPLEMENTARY MATERIALS

Supplementary material for this article is available at http://advances.sciencemag.org/cgi/content/full/5/6/eaaw5685/DC1

Supplementary Text

Section S1. Primary physical properties of MBi_2Te_4

Section S2. Quantum confinement effects on side surfaces

Fig. S1. Band structures of monolayer MBi_2Te_4 calculated by DFT-HSE excluding SOC.

Fig. S2. Band structures of monolayer MBi_2Te_4 calculated by DFT-HSE including SOC.

Fig. S3. Phonon dispersions of monolayer MBi_2Te_4.

Fig. S4. Band structures of AFM MBi_2Te_4 bulks calculated by the GGA+*U* method with SOC.

Fig. S5. Topological surface states and spin textures for the side (110) surfaces of AFM $MnBi_2Te_4$.

Fig. S6. Band structure and edge states of the four-layer AFM MBi_2Te_4.

Table S1. Physical properties of monolayer MBi_2Te_4 for varying elements M.

Table S2. Physical properties of bulk MBi_2Te_4 for varying elements M.

REFERENCES AND NOTES

1. M. Z. Hasan, C. L. Kane, Colloquium: Topological insulators. *Rev. Mod. Phys.* **82**, 3045 (2010).
2. X.-L. Qi, S.-C. Zhang, Topological insulators and superconductors. *Rev. Mod. Phys.* **83**, 1057 (2011).
3. F. D. M. Haldane, Model for a quantum Hall effect without Landau levels: Condensed-matter realization of the "parity anomaly". *Phys. Rev. Lett.* **61**, 2015–2018 (1988).
4. R. Yu, W. Zhang, H.-J. Zhang, S.-C. Zhang, X. Dai, Z. Fang, Quantized anomalous Hall effect in magnetic topological insulators. *Science* **329**, 61–64 (2010).
5. C.-Z. Chang, J. Zhang, X. Feng, J. Shen, Z. Zhang, M. Guo, K. Li, Y. Ou, P. Wei, L.-L. Wang, Z.-Q. Ji, Y. Feng, S. Ji, X. Chen, J. Jia, X. Dai, Z. Fang, S.-C. Zhang, K. He, Y. Wang, L. Lu, X.-C. Ma, Q.-K. Xue, Experimental observation of the quantum anomalous Hall effect in a magnetic topological insulator. *Science* **340**, 167–170 (2013).
6. C.-Z. Chang, W. Zhao, D. Y. Kim, H. Zhang, B. A. Assaf, D. Heiman, S.-C. Zhang, C. Liu, M. H. Chan, J. S. Moodera, High-precision realization of robust quantum anomalous Hall state in a hard ferromagnetic topological insulator. *Nat. Mater.* **14**, 473–477 (2015).
7. X.-L. Qi, T. L. Hughes, S.-C. Zhang, Topological field theory of time-reversal invariant insulators. *Phys. Rev. B* **78**, 195424 (2008).
8. F. Wilczek, Two applications of axion electrodynamics. *Phys. Rev. Lett.* **58**, 1799–1802 (1987).
9. A. M. Essin, J. E. Moore, D. Vanderbilt, Magnetoelectric polarizability and axion electrodynamics in crystalline insulators. *Phys. Rev. Lett.* **102**, 146805 (2009).
10. R. S. K. Mong, A. M. Essin, J. E. Moore, Antiferromagnetic topological insulators. *Phys. Rev. B* **81**, 245209 (2010).
11. Q. L. He, L. Pan, A. L. Stern, E. C. Burks, X. Che, G. Yin, J. Wang, B. Lian, Q. Zhou, E. S. Choi, K. Murata, X. Kou, Z. Chen, T. Nie, Q. Shao, Y. Fan, S.-C. Zhang, K. Liu, J. Xia, K. L. Wang, Chiral Majorana fermion modes in a quantum anomalous Hall insulator–superconductor structure. *Science* **357**, 294–299 (2017).
12. Y. Jin, R. Wang, B. Xia, B. Zheng, H. Xu, Three-dimensional quantum anomalous Hall effect in ferromagnetic insulators. *Phys. Rev. B* **98**, 081101 (2018).
13. Y. Xu, B. Yan, H.-J. Zhang, J. Wang, G. Xu, P. Tang, W. Duan, S.-C. Zhang, Large-gap quantum spin Hall insulators in tin films. *Phys. Rev. Lett.* **111**, 136804 (2013).
14. Y. Xu, Z. Gan, S.-C. Zhang, Enhanced thermoelectric performance and anomalous Seebeck effects in topological insulators. *Phys. Rev. Lett.* **112**, 226801 (2014).
15. F.-f. Zhu, W.-j. Chen, Y. Xu, C.-l. Gao, D.-d. Guan, C.-h. Liu, D. Qian, S.-C. Zhang, J.-f. Jia, Epitaxial growth of two-dimensional stanene. *Nat. Mater.* **14**, 1020–1025 (2015).
16. A. Molle, J. Goldberger, M. Houssa, Y. Xu, S.-C. Zhang, D. Akinwande, Buckled two-dimensional Xene sheets. *Nat. Mater.* **16**, 163–169 (2017).
17. X. Wan, A. M. Turner, A. Vishwanath, S. Y. Savrasov, Topological semimetal and Fermi-arc surface states in the electronic structure of pyrochlore iridates. *Phys. Rev. B* **83**, 205101 (2011).
18. G. Xu, H. Weng, Z. Wang, X. Dai, Z. Fang, Chern semimetal and the quantized anomalous Hall effect in $HgCr_2Se_4$. *Phys. Rev. Lett.* **107**, 186806 (2011).
19. H. Weng, C. Fang, Z. Fang, B. A. Bernevig, X. Dai, Weyl semimetal phase in noncentrosymmetric transition-metal monophosphides. *Phys. Rev. X* **5**, 011029 (2015).
20. S.-Y. Xu, I. Belopolski, N. Alidoust, M. Neupane, G. Bian, C. Zhang, R. Sankar, G. Chang, Z. Yuan, C.-C. Lee, S.-M. Huang, H. Zheng, J. Ma, D. S. Sanchez, B. K. Wang, A. Bansil, F. Chou, P. P. Shibayev, H. Lin, S. Jia, M. Z. Hasan, Discovery of a Weyl fermion semimetal and topological Fermi arcs. *Science* **349**, 613–617 (2015).
21. A. A. Soluyanov, D. Gresch, Z. Wang, Q. Wu, M. Troyer, X. Dai, B. A. Bernevig, Type-II Weyl semimetals. *Nature* **527**, 495–498 (2015).
22. P. Tang, Q. Zhou, G. Xu, S.-C. Zhang, Dirac fermions in an antiferromagnetic semimetal. *Nat. Phys.* **12**, 1100–1104 (2016).
23. G. Hua, S. Nie, Z. Song, R. Yu, G. Xu, K. Yao, Dirac semimetal in type-IV magnetic space groups. *Phys. Rev. B* **98**, 201116 (2018).
24. F. Katmis, V. Lauter, F. S. Nogueira, B. A. Assaf, M. E. Jamer, P. Wei, B. Satpati, J. W. Freeland, I. Eremin, D. Heiman, P. Jarillo-Herrero, J. S. Moodera, A high-temperature ferromagnetic topological insulating phase by proximity coupling. *Nature* **533**, 513–516 (2016).
25. M. Mogi, M. Kawamura, R. Yoshimi, A. Tsukazaki, Y. Kozuka, N. Shirakawa, K. S. Takahashi, M. Kawasaki, Y. Tokura, A magnetic heterostructure of topological insulators as a candidate for an axion insulator. *Nat. Mater.* **16**, 516–521 (2017).
26. M. Mogi, M. Kawamura, A. Tsukazaki, R. Yoshimi, K. S. Takahashi, M. Kawasaki, Y. Tokura, Tailoring tricolor structure of magnetic topological insulator for robust axion insulator. *Sci. Adv.* **3**, eaao1669 (2017).
27. D. Xiao, J. Jiang, J.-H. Shin, W. Wang, F. Wang, Y.-F. Zhao, C. Liu, W. Wu, M. H. W. Chan, N. Samarth, C.-Z. Chang, Realization of the axion insulator state in quantum anomalous Hall sandwich heterostructures. *Phys. Rev. Lett.* **120**, 056801 (2018).
28. E. O. Lachman, A. F. Young, A. Richardella, J. Cuppens, H. R. Naren, Y. Anahory, A. Y. Meltzer, A. Kandala, S. Kempinger, Y. Myasoedov, M. E. Huber, N. Samarth, E. Zeldov, Visualization of superparamagnetic dynamics in magnetic topological insulators. *Sci. Adv.* **1**, e1500740 (2015).
29. E. O. Lachman, M. Mogi, J. Sarkar, A. Uri, K. Bagani, Y. Anahory, Y. Myasoedov, M. E. Huber, A. Tsukazaki, M. Kawasaki, Y. Tokura, E. Zeldov, Observation of superparamagnetism in coexistence with quantum anomalous Hall C = ±1 and C = 0 Chern states. *npj Quantum Mater.* **2**, 70 (2017).
30. M. M. Otrokov, T. V. Menshchikova, M. G. Vergniory, I. P. Rusinov, A. Y. Vyazovskaya, Y. M. Koroteev, G. Bihlmayer, A. Ernst, P. M. Echenique, A. Arnau, E. V. Chulkov, Highly-ordered wide bandgap materials for quantized anomalous Hall and magnetoelectric effects. *2D Mater.* **4**, 025082 (2017).
31. M. M. Otrokov, T. V. Menshchikova, I. P. Rusinov, M. G. Vergniory, V. M. Kuznetsov, E. V. Chulkov, Magnetic extension as an efficient method for realizing the quantum anomalous hall state in topological insulators. *JETP Lett.* **105**, 297–302 (2017).
32. A. K. Geim, I. V. Grigorieva, Van der Waals heterostructures. *Nature* **499**, 419–425 (2013).
33. H. Zhang, C.-X. Liu, X.-L. Qi, X. Dai, Z. Fang, S.-C. Zhang, Topological insulators in Bi_2Se_3, Bi_2Te_3 and Sb_2Te_3 with a single Dirac cone on the surface. *Nat. Phys.* **5**, 438–442 (2009).
34. X. Qian, J. Liu, L. Fu, J. Li, Quantum spin Hall effect in two-dimensional transition metal dichalcogenides. *Science* **346**, 1344–1347 (2014).
35. B. Huang, G. Clark, E. Navarro-Moratalla, D. R. Klein, R. Cheng, K. L. Seyler, D. Zhong, E. Schmidgall, M. A. McGuire, D. H. Cobden, W. Yao, D. Xiao, P. Jarillo-Herrero, X. Xu, Layer-dependent ferromagnetism in a van der Waals crystal down to the monolayer limit. *Nature* **546**, 270–273 (2017).
36. C. Gong, L. Li, Z. Li, H. Ji, A. Stern, Y. Xia, T. Cao, W. Bao, C. Wang, Y. Wang, Z. Q. Qiu, R. J. Cava, S. G. Louie, J. Xia, X. Zhang, Discovery of intrinsic ferromagnetism in two-dimensional van der Waals crystals. *Nature* **546**, 265–269 (2017).
37. C. L. Kane, E. J. Mele, Quantum spin Hall effect in graphene. *Phys. Rev. Lett.* **95**, 226801 (2005).
38. B. A. Bernevig, T. L. Hughes, S.-C. Zhang, Quantum spin Hall effect and topological phase transition in HgTe quantum wells. *Science* **314**, 1757–1761 (2006).
39. M. König, S. Wiedmann, C. Brüne, A. Roth, H. Buhmann, L. W. Molenkamp, X.-L. Qi, S.-C. Zhang, Quantum spin Hall insulator state in HgTe quantum wells. *Science* **318**, 766–770 (2007).
40. D. S. Lee, T.-H. Kim, C.-H. Park, C.-Y. Chung, Y. S. Lim, W.-S. Seo, H.-H. Park, Crystal structure, properties and nanostructuring of a new layered chalcogenide semiconductor, Bi_2MnTe_4. *CrstEngComm* **15**, 5532–5538 (2013).
41. Y. Gong, J. Guo, J. Li, K. Zhu, M. Liao, X. Liu, Q. Zhang, L. Gu, L. Tang, X. Feng, D. Zhang, W. Li, C. L. Song, L. L. Wang, P. Yu, X. Chen, Y. Y. Wang, H. Yao, W. H. Wen, Y. Xu, S.-C. Zhang, X. C. Ma, Q.-K. Xue, K. He, Experimental realization of an intrinsic magnetic topological insulator. arXiv:1809.07926 [cond-mat.mtrl-sci] (21 September 2018).
42. S. V. Eremeev, M. M. Otrokov, E. V. Chulkov, Competing rhombohedral and monoclinic crystal structures in $MnPn_2Ch_4$ compounds: An ab-initio study. *J. Alloys Compd.* **709**, 172–178 (2017).
43. L. Fu, C. L. Kane, Topological insulators with inversion symmetry. *Phys. Rev. B* **76**, 045302 (2007).
44. L. Wu, M. Salehi, N. Koirala, J. Moon, S. Oh, N. P. Armitage, Quantized Faraday and Kerr rotation and axion electrodynamics of a 3D topological insulator. *Science* **354**, 1124–1127 (2016).
45. D. Hsieh, D. Qian, L. Wray, Y. Xia, Y. S. Hor, R. J. Cava, M. Z. Hasan, A topological Dirac insulator in a quantum spin Hall phase. *Nature* **452**, 970–974 (2008).
46. D. Hsieh, Y. Xia, L. Wray, D. Qian, A. Pal, J. H. Dil, J. Osterwalder, F. Meier, G. Bihlmayer, C. L. Kane, Y. S. Hor, R. J. Cava, M. Z. Hasan, Observation of unconventional quantum spin textures in topological insulators. *Science* **323**, 919–922 (2009).
47. D. Zhang, M. Shi, K. He, D. Xing, H. Zhang, J. Wang, Topological axion states in magnetic insulator $MnBi_2Te_4$ with the quantized magnetoelectric effect. arXiv:1808.08014 [cond-mat.mes-hall] (24 August 2018).
48. M. M. Otrokov, I. I. Klimovskikh, H. Bentmann, A. Zeugner, Z. S. Aliev, S. Gass, A. U. B. Wolter, A. V. Koroleva, D. Estyunin, A. M. Shikin, M. Blanco-Rey, M. Hoffmann, A. Y. Vyazovskaya, S. V. Eremeev, Y. M. Koroteev, I. R. Amiraslanov, M. B. Babanly, N. T. Mamedov, N. A. Abdullayev, V. N. Zverev, B. Buchner, E. F. Schwier, S. Kumar, A. Kimura, L. Petaccia, G. D. Santo, R. C. Vidal, S. Schatz, K. Kißner, C.-H. Min, S. K. Moser, T. R. F. Peixoto, F. Reinert, A. Ernst, P. M. Echenique, A. Isaeva, E. V. Chulkov, Prediction and observation of the first antiferromagnetic topological insulator. arXiv:1809.07389 [cond-mat.mtrl-sci] (19 September 2018).
49. M. M. Otrokov, I. P. Rusinov, M. Blanco-Rey, M. Hoffmann, A. Y. Vyazovskaya, S. V. Eremeev, A. Ernst, P. M. Echenique, A. Arnau, E. V. Chulkov, Unique thickness-dependent properties of the van der Waals interlayer antiferromagnet $MnBi_2Te_4$ films. *Phys. Rev. Lett.* **122**, 107202 (2018).
50. S. Chowdhury, K. F. Garrity, F. Tavazza, Prediction of Weyl semimetal, AFM topological insulator, nodal line semimetal, and Chern insulator phases in Bi_2MnSe_4. *npj Comput. Mater.* **5**, 33 (2018).
51. S. H. Lee, Y. Zhu, Y. Wang, L. Miao, T. Pillsbury, S. Kempinger, D. Graf, N. Alem, C.-Z. Chang, N. Samarth, Z. Mao, Spin scattering and noncollinear spin structure-induced intrinsic anomalous Hall effect in antiferromagnetic topological insulator $MnBi_2Te_4$. arXiv:1812.00339 [cond-mat.mtrl-sci] (2 December 2018).
52. Y. Peng, Y. Xu, Proximity-induced Majorana hinge modes in antiferromagnetic topological insulators. arXiv:1809.09112 [cond-mat.mes-hall] (24 September 2018).

53. G. Kresse, J. Furthmüller, Efficient iterative schemes for ab initio total-energy calculations using a plane-wave basis set. *Phys. Rev. B* **54**, 11169–11186 (1996).
54. J. P. Perdew, K. Burke, M. Ernzerhof, Generalized gradient approximation made simple. *Phys. Rev. Lett.* **77**, 3865–3868 (1996).
55. A. V. Krukau, O. A. Vydrov, A. F. Izmaylov, G. E. Scuseria, Influence of the exchange screening parameter on the performance of screened hybrid functionals. *J. Chem. Phys.* **125**, 224106 (2006).
56. A. D. Becke, E. R. Johnson, A simple effective potential for exchange. *J. Chem. Phys.* **124**, 221101 (2006).
57. S. Grimme, J. Antony, S. Ehrlich, H. Krieg, A consistent and accurate ab initio parametrization of density functional dispersion correction (DFT-D) for the 94 elements H-Pu. *J. Chem. Phys.* **132**, 154104 (2010).
58. V. Blum, R. Gehrke, F. Hanke, P. Havu, V. Havu, X. Ren, K. Reuter, M. Scheffler, Ab initio molecular simulations with numeric atom-centered orbitals. *Comput. Phys. Commun.* **180**, 2175–2196 (2009).
59. Q. Wu, S. Zhang, H.-F. Song, M. Troyer, A. A. Soluyanov, WannierTools: An open-source software package for novel topological materials. *Comput. Phys. Commun.* **224**, 405–416 (2018).

Acknowledgments
Funding: This work was supported by the Basic Science Center Project of NSFC (grant no. 51788104), the Ministry of Science and Technology of China (grant nos. 2016YFA0301001, 2018YFA0307100, 2018YFA0305603, and 2017YFA0303303), the National Natural Science Foundation of China (grant nos. 11674188, 11334006, 11874035, and 51661135024), and the Beijing Advanced Innovation Center for Future Chip (ICFC). Y.X. acknowledges support from the National Thousand Young Talents Program and Tsinghua University Initiative Scientific Research Program. **Author contributions:** Y.X., W.D., and K.H. conceived the project. J.L. performed the first-principles calculations with the help of Y.L., S.D., and Z.W. Y.X., W.D., K.H., B.-L.G., and S.-C.Z. analyzed the data. Y.X. wrote the manuscript with input from J.L., W.D., K.H., B.-L.G., and S.-C.Z. All authors discussed the results and commented on the manuscript. **Competing interests:** The authors declare that they have no competing interests. **Data and materials availability:** All data needed to evaluate the conclusions in the paper are present in the paper and/or the Supplementary Materials. Additional data related to this paper may be requested from the authors.

Submitted 6 January 2019
Accepted 10 May 2019
Published 14 June 2019
10.1126/sciadv.aaw5685

Citation: J. Li, Y. Li, S. Du, Z. Wang, B.-L. Gu, S.-C. Zhang, K. He, W. Duan, Y. Xu, Intrinsic magnetic topological insulators in van der Waals layered $MnBi_2Te_4$-family materials. *Sci. Adv.* **5**, eaaw5685 (2019).